The Astrophysical Journal, 659:1241–1256, 2007 April 20

PHOTOMETRIC STELLAR VARIABILITY IN THE GALACTIC CENTER

M. Rafelski, A. M. Ghez,[1] S. D. Hornstein, J. R. Lu, and M. Morris
Division of Astronomy and Astrophysics, University of California, Los Angeles, CA 90095-1547; marcar@astro.ucla.edu, ghez@astro.ucla.edu, seth@astro.ucla.edu, jlu@astro.ucla.edu, morris@astro.ucla.edu
Received 2006 October 6; accepted 2006 December 19

ABSTRACT

We report the results of a diffraction-limited, photometric variability study of the central $5'' \times 5''$ of the Galaxy conducted over the past 10 years using speckle imaging techniques on the W. M. Keck I 10 m telescope. Within our limiting magnitude of $m_K < 16$ mag for images made from a single night of data, we find a minimum of 15 K[2.2 μm]-band variable stars out of 131 monitored stars. The only periodic source in our sample is the previously identified variable IRS 16SW, for which we measure an orbital period of 19.448 ± 0.002 days. In contrast to recent results, our data on IRS 16SW show an asymmetric phased light curve with a much steeper fall time than rise time, which may be due to tidal deformations caused by the proximity of the stars in their orbits. We also identify a possible wind colliding binary (IRS 29N) based on its photometric variation over a few year timescale, which is likely due to episodic dust production. None of the four luminous blue variable (LBV) candidates in our sample show the characteristic large increase or decrease in luminosity. However, our time baseline is too short to rule them out as LBVs. Among the remaining variable stars, the majority are early-type stars, and three are possibly variable due to line-of-sight extinction variations. For the seven OB stars at the center of our field of view that have well-determined three-dimensional orbits, we see no evidence of flares or dimming of their light, which limits the possibility of a cold, geometrically thin, inactive accretion disk around the supermassive black hole, Sgr A*.

Subject headings: Galaxy: center — infrared: stars — stars: variables: other

1. INTRODUCTION

The stellar cluster at the Galactic center (GC) presents a unique opportunity to study the evolution and properties of stars within the sphere of influence of a $(3-4) \times 10^6\ M_\odot$ supermassive black hole (SMBH) (Ghez et al. 2003, 2005a; Schödel et al. 2003). Photometric variability offers a useful approach to a number of outstanding questions regarding this stellar population, which is composed of a mixture of old giants and young, massive stars. (Krabbe et al. 1991, 1995; Blum et al. 1996a, 1996b, 2003; Figer et al. 2003; Paumard et al. 2001, 2004a, 2006). For example, light curves can easily reveal close binary stars, which are relevant in several ways to our understanding of stars at the Galactic center.

First, binaries on radial orbits that are disrupted by the central black hole may provide a mechanism for capturing young stars from large galactocentric radii, where the conditions are conducive to star formation, and retaining them at the smaller, less hospitable radii where many young stars are found today (Gould & Quillen 2003). Second, binary companions may facilitate the production of dust around the WC subclass of Wolf-Rayet stars, which are massive post-main-sequence stars undergoing rapid mass loss. While conditions in the hostile environment (high temperatures in particular) of the stellar winds do not favor the formation of dust (Williams et al. 1987), compression within wind-colliding binary systems could overcome this challenge (White & Becker 1995; Veen et al. 1998; Williams & van der Hucht 2000; Lefèvre et al. 2005). Third, binaries provide a direct measurement of stellar masses. This is especially helpful for the most massive stars in the Galactic center, as it would assist our understanding of the recent star formation history.

Another way in which a photometric variability study constrains the recent star formation history, as well as our understanding of massive star evolution, is the possibility of identifying luminous blue variables (LBVs). There are currently only 12 confirmed Galactic LBVs and 23 additional candidates, with six candidates in the Galactic center IRS 16 cluster of stars alone (Clark et al. 2005). The LBV phase plays an important, although poorly constrained, role in stellar evolution, because, during this phase, stars experience significant mass loss, with rates of $\sim 10^{-2}\ M_\odot\ \mathrm{yr}^{-1}$ during eruptions and as high as $10^{-4.5}\ M_\odot\ \mathrm{yr}^{-1}$ during quiescent phases (Abbott & Conti 1987; Humphreys & Davidson 1994; Massey 2003). From a star formation history standpoint, the LBV phase is notable because it is the first of several post-main-sequence phases that only the most massive stars ($M \gtrsim 60-85\ M_\odot$) may go through before becoming supernovae. Stars stay in this phase for only $\sim 10^4$ yr (Stothers & Chin 1996) before entering the Wolf-Rayet phase, which typically lasts a few times 10^6 yr (Meynet & Maeder 2005). Less massive stars ($M \gtrsim 40\ M_\odot$) will skip the LBV phase and become Wolf-Rayet (W-R) stars, but on timescales longer than that of the more massive stars that experienced an LBV phase. Therefore, in principle, the numbers of LBVs and W-R stars can constrain recent star formation histories (e.g., Paumard et al. 2006; Figer 2004). In this context the candidate LBVs at the Galactic center are perplexing in the context of the $\gtrsim$25 W-R stars located in their immediate vicinity, since in a single starburst event one would not expect to see any W-R stars if the most massive stars are just now evolving through the LBV phase. This is similar to the problem posed by the presence of two LBVs in the Quintuplet cluster (Figer 2004). If confirmed, the LBV candidates would suggest that this region has undergone multiple recent star-forming events, or that our understanding of LBV evolution is incomplete.

The photometry of stars in close proximity to the SMBH can also be used to constrain the properties of a possible cold, geometrically thin, inactive accretion disk around Sgr A*, which

[1] Institute of Geophysics and Planetary Physics, University of California, Los Angeles, CA 90095-1565.

could explain the present-day low luminosity of Sgr A* (Nayakshin & Sunyaev 2003; Cuadra et al. 2003). In the presence of such a disk, we would expect to see nearby stars eclipsed or reddened when they pass behind the disk.

Very few photometric variable studies of the Galactic center exist. Tamura et al. (1996) introduced the idea that stars close to the Galactic center are expected to have a higher fraction of ellipsoidal[2] and eclipsing variable binaries than the stars in the solar neighborhood, but found very few variable stars and no binary stars. Seeing-limited studies (Tamura et al. 1996; Blum et al. 1996a) are limited to the brightest stars, due to stellar confusion caused by the high stellar densities and proper motions close to the central black hole. With high angular resolution data, Ott et al. (1999) have identified the only known eclipsing binary system in this region (see also DePoy et al. 2004; Martins et al. 2006). Furthermore, they suggest that as much as half of their sample ($K \lesssim 13$) may be variable. However, the variability fraction decreases at smaller galactocentric radii starting from $\sim 5''$, suggesting that even at a high resolution of $0.13''$ their sensitivity to variability is limited by stellar confusion.

In this paper, we present the results of a stellar variability study of the central $5'' \times 5''$ of our Galaxy, based on 10 yr of $K[2.2\ \mu\mathrm{m}]$ diffraction-limited images from the W. M. Keck I telescope ($\theta = 0.05''$). The observations are described in § 2 and the data and methodology to determine variability in § 3. We discuss the variable star population in § 4, which includes identification of asymmetries in the light curve of the eclipsing binary star IRS 16SW and the discovery of a likely wind colliding binary star in IRS 29N, and summarize our major findings in § 5.

2. OBSERVATIONS

K-band ($\lambda_0 = 2.2\ \mu$m, $\Delta\lambda = 0.4\ \mu$m) speckle imaging observations of the Galaxy's central stellar cluster were obtained with the W. M. Keck I 10 m telescope using the facility near-infrared camera (NIRC; Matthews & Soifer 1994). Observations taken from 1995 to 2004 have been described in detail elsewhere (Ghez et al. 1998, 2000, 2005a; Lu et al. 2005), and new observations on 2005 April 24–25 were conducted in a similar manner, resulting in diffraction-limited images. Each night several thousand short-exposure frames were taken in sets of $\sim$200, with NIRC in its fine plate scale mode, which has a scale of 20.40 ± 0.04 mas pixel^{-1} and a corresponding field of view (FOV) of $5.22'' \times 5.22''$ (Matthews et al. 1996). Table 1 lists the date and number of frames obtained for each of the 50 nights of observations used in this study.

3. DATA ANALYSIS AND RESULTS

3.1. *Image Processing*

The individual frames are processed in two steps to create a final average image for each night of observation. First, the standard image reduction steps of sky subtraction, flat fielding, bad pixel correction, optical distortion correction,[3] and pixel magnification by a factor of 2 are carried out on each frame. Second, the frames from each night of observation are combined using the method of "shift-and-add" (Christou 1991) with the frame selection and weighting scheme prescribed by Hornstein (2006). In short, each frame is analyzed for Strehl quality using the peak pixel value of IRS 16C, and low-quality frames, which do not improve the cumulative signal-to-noise ratio (S/N) for the observations from each night, are rejected. This typically leaves $\sim$1600 frames for each night or 37% of the original data set (see col. [3] of Table 1). The remaining frames for a given night are combined with shift-and-add in an average that is weighted by each frame's peak pixel value for IRS 16C. The final images have typical Strehl ratios of $\sim$0.07 (see col. [8] of Table 1). The data set from each night is also divided into three equivalent quality (and randomized in time) subsets to make three independent weighted shift-and-add image subsets, which are used to determine measurement uncertainties and to reject spurious sources.

Sources are identified in individual images and cross-identified between images using the strategy developed in Ghez et al. (1998, 2000, 2005a) and J. R. Lu et al. (2007, in preparation), which for this study entails four separate steps. In the first step of the source identification process, we generate a conservative initial list of sources for each night of data to help minimize spurious source detection. This is done using the point-spread function (PSF) fitting routine StarFinder (Diolaiti et al. 2000) to identify sources in both the average images and the subset images. StarFinder identifies sources through cross-correlation of each image with its PSF model, which, for our implementation, is generated from the two bright stars IRS 16C and IRS 16NW. The initial source list for each night of data is composed of only sources detected in the average images with correlation values above 0.8 and in all three subset images with correlation values above 0.6. In the second step of the source identification process, the source lists from all nights are cross-identified to produce a master list of sources, using a process that is described in Ghez et al. (1998) and that also solves for the sources' proper motions. To further ensure that no spurious sources have been detected, we require that sources be detected in a minimum of 13 nights.[4] Figure 1 displays the 131 sources contained in our final master list. In the third step of the source identification process, we return to the original images to search more aggressively for the sources on the master list that were missed in some of the images. We explicitly feed the master list of sources into StarFinder and search for only these sources at their predicted positions with more lenient criteria, which require correlation values above 0.4 for both average and subset images. In the fourth and final step, we impose a restriction on our source detections to ensure photometric reliability: we exclude source detections that occur in regions of the average images covered by less than 50% frames that went into making a particular image. These regions, which are on the edges of the image, have relatively low S/N, and the PSFs in these regions may not be well represented by the PSF model. We also exclude individual measurements in which known stars are blended with each other (i.e., sources as listed in Ghez et al. [2005a] as well as Sgr A* IR.) This procedure, in its entirety, produces 4795 detections among 131 sources, which range in m_K magnitude from 9.0 to 16.1 mag (see Fig. 2).

Photometric zero points are established on the basis of the work done by Blum et al. (1996a). While we share seven stars in common with Blum et al. (1996a) (IRS 16NW, 16SW, 16C, 16NE, 29N, 29S, and 16CC), only IRS 16C ($m_K = 9.83 \pm 0.05$ mag) is a suitable photometric reference source. IRS 16SW is a known variable star in the *K* band (Ott et al. 1999; DePoy et al. 2004), and IRS 29N is noted as possibly variable in Hornstein et al.

[2] Ellipsoidal variables are noneclipsing binaries that are elongated by mutual tidal forces (Sterken & Jaschek 1996).

[3] See http://www.keck.hawaii.edu/inst/nirc/distortion.html.

[4] The threshold for the minimum number of nights was chosen by looking for a drop in the distribution of the number of nights that the sources were detected in the first pass at source identification. A minor drop is seen at 13 nights. The final results are not very sensitive to this choice, and we therefore have made a fairly conservative choice.

TABLE 1
List of Observations

Date	Frames[a] (Obs.)	Frames[b] (Used)	Number of Stars[c] (Initial)	Number of Stars[d] (Final)	S/N[e]	Strehl
1995 Jun 10	1200	425	54	66	10.3	0.08
1995 Jun 11	2700	1604	95	110	15.0	0.06
1995 Jun 12	2100	1082	107	108	12.0	0.04
1996 Jun 26	4200	585	116	119	19.8	0.04
1996 Jun 27	2300	1260	117	121	20.5	0.04
1997 May 14	3600	1851	63	82	16.7	0.06
1998 Apr 02	2660	1649	119	121	16.3	0.05
1998 May 14	4560	1748	96	114	16.7	0.04
1998 May 15	7030	1953	41	55	9.9	0.06
1998 Jul 04	2280	943	108	114	17.8	0.08
1998 Aug 04	6270	1469	87	107	15.5	0.05
1998 Aug 05	5700	1592	94	103	17.3	0.07
1998 Oct 09	2660	1188	83	99	17.1	0.08
1998 Oct 11	570	450	79	96	15.0	0.05
1999 May 02	7030	1589	115	116	19.9	0.09
1999 May 03	2090	1264	103	114	16.0	0.07
1999 Jul 24	5510	2239	113	119	18.5	0.11
1999 Jul 25	950	788	102	114	15.0	0.06
2000 Apr 21	3040	947	90	112	18.5	0.04
2000 May 19	9880	1970	64	91	10.2	0.09
2000 May 20	7600	2146	81	97	16.5	0.10
2000 Jul 19	8740	1939	111	116	17.1	0.07
2000 Jul 20	3420	1454	111	119	19.8	0.09
2000 Oct 18	2280	1807	82	107	15.1	0.05
2001 May 08	1520	889	111	124	20.1	0.04
2001 May 09	6270	1990	76	100	13.1	0.08
2001 Jul 28	4180	1752	99	104	20.0	0.13
2001 Jul 29	6080	1751	105	115	19.0	0.07
2002 Apr 23	7410	1669	117	119	17.2	0.05
2002 Apr 24	7790	1882	104	113	19.6	0.06
2002 May 23	1900	1249	66	84	18.3	0.07
2002 May 24	2660	1537	85	100	17.7	0.09
2002 May 28	2850	1866	59	80	13.2	0.06
2002 May 29	3420	1552	86	104	16.8	0.07
2002 Jun 01	5510	1992	43	53	7.7	0.09
2002 Jul 19	4370	1115	41	57	7.0	0.07
2002 Jul 20	3990	1355	51	64	11.0	0.06
2003 Apr 21	5130	1799	93	107	19.1	0.04
2003 Apr 23	5320	1970	69	87	13.2	0.05
2003 Jul 22	5130	1718	70	94	16.6	0.08
2003 Sep 07	4560	1795	108	112	16.3	0.07
2003 Sep 08	4370	1223	97	110	12.3	0.07
2004 Apr 29	6840	1181	53	68	14.5	0.11
2004 Apr 30	4180	1203	98	105	16.6	0.05
2004 Jul 25	5320	2007	98	110	18.1	0.08
2004 Jul 26	8550	2309	33	38	6.7	0.08
2004 Aug 29	3230	1328	120	122	21.0	0.10
2005 Apr 24	7410	2195	51	60	11.6	0.07
2005 Apr 25	9500	2035	116	116	20.8	0.05
2005 Jul 26	6650	1497	98	113	19.0	0.06

Note.—All observations are speckle K-band ($\lambda_0 = 2.2$ μm, $\Delta\lambda = 0.4$ μm) images.
[a] The number of frames observed in the night in stacks of 190 frames.
[b] The number of frames used in weighted shift-and-add routine described in Hornstein (2006).
[c] Number of stars in initial source list.
[d] Number of stars in final source list.
[e] The signal-to-noise ratio determined from median uncertainties of the six faintest nonvariable stars detected in all the nights (S0-14, S1-25, S0-13, S1-68, S2-5, and S1-34) with $m_k \sim 13.4$ mag.

(2002). IRS 16CC appears to be variable in the L band; Blum et al. (1996a) list a recalibrated value from Depoy & Sharp (1991) of 8.7 ± 0.2 mag, while Simons & Becklin (1996) measure 10.2 ± 0.2 mag. Among the remaining sources, only IRS 16C is in the final source lists of all the images. Several nonvariable sources (see § 3.2.1) are used a posteriori to confirm that IRS 16C is nonvarying. Specifically, we check for any systematic shifts in the zero points by examining the normalized flux densities $[Q_j = \sum_i^N (\mathrm{flux}_{i,j}/\mathrm{Nflux}_{\mathrm{avg}_i})$, where index i represents each star in an image of epoch j, $\mathrm{flux}_{\mathrm{avg}_i}$ is the weighted average of the

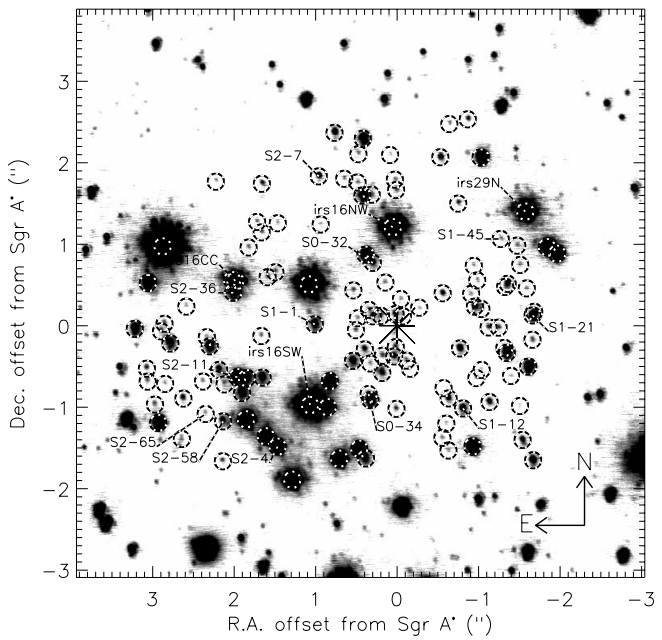

FIG. 1.— Identification of sources from this study overlaid on a $6'' \times 6''$ region of an LGS K''-band ($\lambda_0 = 2.1$ μm) image from A. M. Ghez et al. (2007, in preparation) taken on 2005 June 30. All 131 sources are circled, but only variable sources are labeled. The location of Sgr A* is marked with an asterisk.

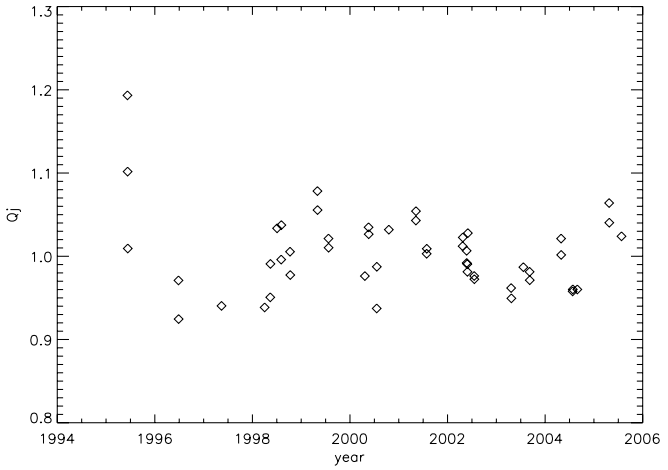

FIG. 3.— Average normalized flux densities (Q_j, as defined in § 3.1) as a function of time. The variations seen are consistent with the measurement uncertainties for bright stars and are therefore demonstrative of the stability of our calibrator IRS 16C. This quantity is used as a scale factor to improve the quality of our relative photometry.

flux for that star over all images, and N is the number of stars used] of the seven least variable bright stars that are identified in all 50 images (S1-3, S1-5, S2-22, S2-5, S1-68, S0-13, and S1-25) (see § 3.2.1). The photometric stability of IRS 16C is shown in Figure 3, which plots Q_j versus the observing dates. The reference source IRS 16C appears to be stable over time, since the standard deviation of Q_j is 0.05, which is consistent with our measurement uncertainty for bright stars. Increasing the number of reference stars to 11 nonvariable sources present in all frames in all 50 nights yields the same result. We therefore conclude that IRS 16C is nonvarying to within our measurement uncertainties and include it in our list of nonvarying sources. Uncertainty in each of our reported relative photometry values is initially estimated as the root mean square (rms) deviation from the average of the measurements from the three different subset images. The rms value is added in quadrature with the uncertainty in the brightness of IRS 16C (0.05 mag) determined from the standard deviation of the normalized flux densities Q_j. As Figure 4 shows, the median uncertainties grow from a floor of about 0.06–0.21 mag for the $K = 16$ mag sources.

3.2. *Variability*

3.2.1. *Identifying Variables*

There is a wide range of methods for testing photometric variability, and the challenge for these various approaches is to avoid declaring a nonvariable source variable on the basis of a few outlying data points (Welch & Stetson 1993). We therefore have chosen to use the Kolmogorov-Smirnov (K-S) test to calculate the probability that a *distribution* of data points is consistent with a model of a distribution of measurements for a nonvariable source. This approach is less sensitive to outlying data points than the commonly used χ^2-test, which is an analysis of a single number description of how well a data set matches a model. In the K-S test, we adopt as our model a nonvariable light curve with Gaussian-distributed uncertainties, and we test the consistency of the measurements with the model. Specifically, we examine the distribution

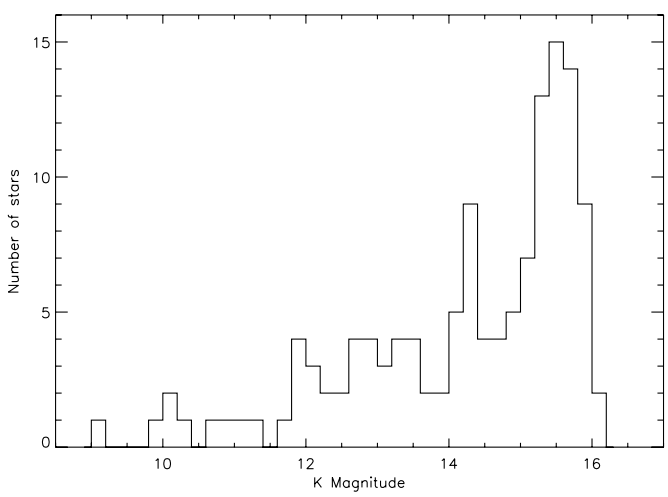

FIG. 2.— An m_K histogram of the 131 stars in our sample, which range in magnitude from 9.0 to 16.1 mag.

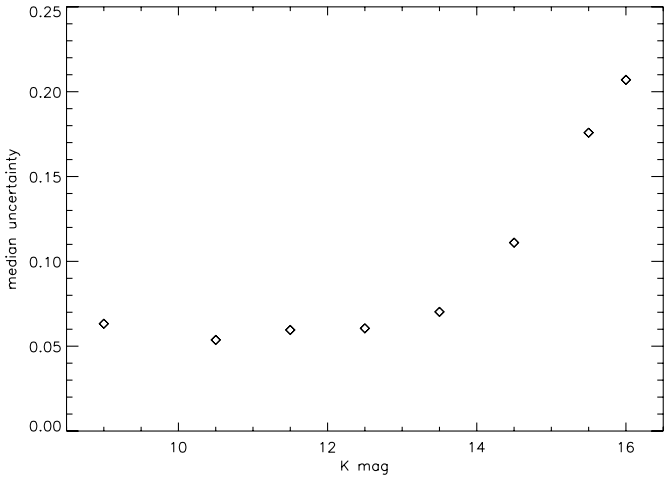

FIG. 4.— Median measurement uncertainty of stars binned by magnitude. The median uncertainties grow from a floor of about 0.06 to 0.21 mag for the $K = 16$ mag sources.

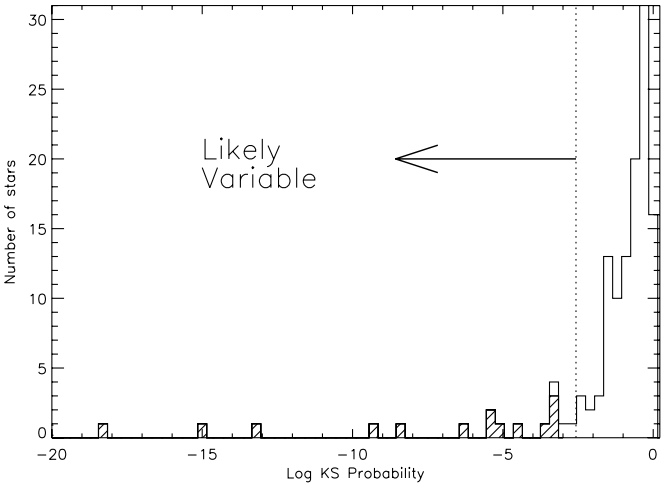

FIG. 5.—K-S test probabilities of all the stars, with low values implying a low probability for a star to be nonvariable. We classify a star as variable if it has a K-S probability of less than 2.7×10^{-3}, which is equivalent to a 3 σ cutoff value for Gaussian distributed uncertainties and is marked by the dashed line. To ensure all our low K-S probability stars are truly variable, we require all variable stars to have positive intrinsic variance. We mark all variable stars identified in this survey with hatches.

of $X_j = \left[(\mathrm{flux}_j - \mathrm{flux}_{\mathrm{avg}})/\sigma_{\mathrm{flux}_j}\right]$, where flux_j is the flux of a star in a image of epoch j, σ_{flux_j} is the corresponding uncertainty, and $\mathrm{flux}_{\mathrm{avg}}$ is the weighted average of the flux for that star over all images. The resulting K-S probabilities, which have allowed values between 0 and 1, describe how likely it is that a source's measurements are consistent with a nonvariable source. Therefore, variable stars, whose intensity variations are larger or comparable to our measurement uncertainties, should have very low K-S probabilities. We classify a star as variable if it has a K-S probability of less than 2.7×10^{-3}, which is the equivalent to a 3 σ cut for Gaussian distributed uncertainties (see Fig. 5). To ensure all our low K-S probability stars are truly variable, we also require these stars to have positive estimates of their intrinsic flux density variance, $\sigma^2_{\mathrm{intrinsic}} = \sigma^2_{\mathrm{measured}} - \langle\delta\rangle^2$, where the first term is the dispersion of the measured flux densities and the second term removes the bias introduced by the measurement uncertainties, δ. At this point, the seven least variable bright stars detected in all images, used in § 3.1 to define Q_j, are identified. We then scale all our photometry by Q_j in order to reduce the fluctuations induced by measurement errors on IRS 16C. The K-S and intrinsic variance tests are then repeated. Tables 2 and 3 list the properties of the variable and nonvariable stars in our sample, respectively, and the light curves of all variable stars and a few key nonvariable stars are shown in Figures 8–13. While there are almost certainly other variable stars that we have excluded, our uncertainties limit our ability to classify more of these stars as variable, especially at the fainter end.

Among the 131 stars in our sample, 15 are identified as photometric variables in K band (see Fig. 1). To this we also add IRS 16CC, known to be variable in the L band (see § 3.1). Since the relative photometric uncertainties are roughly uniform down to a m_K magnitude of $\sim$14 and then grow at fainter magnitudes (see Fig. 4), we report a frequency of variable stars based on the stars brighter than 14 mag. Within this brighter sample of 44 stars, there are 10 variable stars, suggesting a minimum frequency of variable stars of 23%. There is no evidence for radial dependence, suggesting that we are not limited by stellar confusion down to 14 mag.

We compare our results to those of Ott et al. (1999), the only other high spatial resolution study of the variability of sources in

TABLE 2
LIST OF VARIABLE STARS

Star ID	Other ID	K[a] (mag)	Int. Var. (mag)	p (arcsec)	ΔR.A. (arcsec)	ΔDecl. (arcsec)	Probability	Nights (days)	Type
IRS 16SW	E23	10.06 ± 0.19	0.17	1.41	1.04	−0.95	2.3E−23	50	Ofpe/WN9[b,c]
IRS 16NW	E19	10.09 ± 0.09	0.07	1.21	−0.01	1.21	3.3E−05	49	Ofpe/WN9[b,d]
IRS 29N	E31	10.33 ± 0.20	0.18	2.15	−1.63	1.40	1.1E−15	35	WC9[b,d]
IRS 16CC	E27	10.60 ± 0.05	0.01	2.07	1.99	0.57	3.0E−01	50	O9.5-B0.5 I[b,e]
S2-11	GEN+2.03−0.63	11.99 ± 0.13	0.11	2.07	1.99	−0.58	4.9E−19	49	Late[d,f]
S2-4	E28:GEN+1.46−1.49	12.26 ± 0.17	0.15	2.05	1.45	−1.45	6.1E−14	47	B0-0.5 I[b,d]
S1-1	GEN+1.01+0.02	13.00 ± 0.11	0.08	0.98	0.98	0.05	3.6E−04	49	Early[g]
S2-36	...	13.28 ± 0.13	0.12	2.08	2.04	0.43	3.7E−09	48	Early[g]
S1-21	E24:W7	13.33 ± 0.17	0.15	1.69	−1.69	0.13	4.2E−06	42	O9-9.5 III?[b,d]
S1-12	E21:W13	13.82 ± 0.18	0.17	1.31	−0.85	−1.00	4.2E−07	45	OB I?[b]
S2-7	E29:GEN+1.06+1.81	14.06 ± 0.25	0.21	2.09	0.97	1.85	4.2E−10	45	O9-B0[b]
S0-32	...	14.18 ± 0.20	0.15	0.81	0.26	0.77	6.3E−04	49	Early[g]
S2-58	...	14.21 ± 0.14	0.10	2.45	2.17	−1.14	6.8E−04	47	Early[g]
S1-45	...	15.41 ± 0.55	0.28	1.63	−1.28	1.00	6.1E−06	41	Early[g]
S2-65	...	15.83 ± 0.49	0.29	2.57	2.37	−1.00	2.5E−04	29	...
S0-34	...	15.85 ± 0.40	0.31	0.83	0.32	−0.77	4.1E−06	26	...

NOTES.—Photometry is relative to IRS 16C ($m_k = 9.83$ mag). Positions are in arcseconds offset from Sgr A* in 1999.56, and p is the projected distance. The K-S probability is equal to 1 for an ideal nonvariable source, and approaches zero for a very variable source. Other IDs are from Paumard et al. (2006) and Genzel et al. (2000), respectively. We classify IRS 29N as an early-type star according to Paumard et al. (2006), although Figer et al. (2003) classifies it as a late-type star.

[a] The magnitudes are Q_j corrected using seven bright nonvariable stars, and the uncertainties do not include the 5% absolute calibration uncertainties. Comparison to other sources requires adding them in quadrature. Uncertainties are calculated as the standard deviation of the mean.

[b] Spectroscopic identification by Paumard et al. (2006).

[c] Identified as possibly variable by Ott et al. (1999).

[d] Identified as nonvariable by Ott et al. (1999).

[e] IRS 16CC appears to be variable in the L band, as discussed in § 3.1.

[f] Spectroscopic identification by Ott (2003). We denote sources with clear CO or He lines as early and late, respectively.

[g] Identification based on the interpretation by Genzel et al. (2003) of m(CO) index of Ott (2003), where Genzel et al. (2003) identify stars with $m(\mathrm{CO}) \geq 0.04$ as late-type stars and stars with $m(\mathrm{CO}) < 0.04$ as early-type stars.

TABLE 3
LIST OF NONVARIABLE STARS

Star ID	Other ID	K[a] (mag)	p (arcsec)	ΔR.A. (arcsec)	ΔDecl. (arcsec)	Nights (days)	Type
IRS 16NE	E39	9.00 ± 0.05	3.06	2.85	1.10	35	Ofpe/WN9[b,c]
IRS 16C	E20	9.83 ± 0.05	1.23	1.13	0.50	50	Ofpe/WN9[b,c,d]
S2-17	E34:GEN+1.27−1.87	10.90 ± 0.07	2.23	1.27	−1.84	35	B0.5-1 I[b,c]
IRS 16SW-E	E32:16SE1	11.00 ± 0.08	2.15	1.85	−1.11	50	WC8/9[b,c]
IRS 29S	...	11.31 ± 0.06	2.08	−1.86	0.93	30	K3 III[e]
S1-24	E26:GEN+0.76−1.55	11.64 ± 0.07	1.72	0.73	−1.55	45	O8-9.5 I[b,c]
S2-16	E35:29NE1	11.85 ± 0.08	2.29	−1.01	2.05	33	WC8/9[b,c]
S1-23	GEN−0.90−1.46	11.86 ± 0.09	1.73	−0.92	−1.46	33	Late[c,f]
S3-2	GEN+3.07+0.56	12.00 ± 0.11	3.09	3.03	0.60	31	Early[g]
S2-6	E30:GEN+1.60−1.36	12.06 ± 0.08	2.07	1.59	−1.31	50	O8.5-9.5 I[b]
S1-3[h]	E15:GEN+0.57+0.84	12.10 ± 0.06	0.99	0.46	0.88	50	Early[g,i]
S3-5	E40:16SE	12.15 ± 0.09	3.16	2.95	−1.13	21	WN5/6[b,c]
S2-8	W2	12.24 ± 0.08	2.16	−1.99	0.84	23	Early[g]
S1-17	GEN+0.55−1.45	12.51 ± 0.08	1.52	0.50	−1.44	49	Late[c,f]
S1-4	GEN+0.77−0.71	12.53 ± 0.07	1.02	0.77	−0.66	50	Early[g]
S2-19	E36:GEN+0.53+2.27	12.62 ± 0.11	2.34	0.42	2.30	33	O9-B0 I?[b,c]
S1-20	GEN+0.41+1.59	12.70 ± 0.11	1.66	0.37	1.61	49	Late[c,f]
S1-22	E25:W14	12.72 ± 0.08	1.72	−1.65	−0.51	42	O8.5-9.5 I?[b,c]
S1-5[h]	GEN+0.43−0.96	12.78 ± 0.04	0.98	0.37	−0.91	50	Late[c,f]
S1-14	E22:W10	12.82 ± 0.07	1.40	−1.37	−0.30	46	O8-9.5 III/I[b,c]
S3-6	GEN+3.26+0.08	12.82 ± 0.05	3.22	3.22	0.09	17	Late[c,f]
S2-22[h]	GEN+2.37−0.29	12.92 ± 0.04	2.33	2.32	−0.22	50	Late[c,f]
S2-38	...	12.93 ± 0.09	2.12	2.04	0.58	44	Late[g]
S2-31	GEN+2.91−0.20	13.06 ± 0.10	2.84	2.83	−0.15	42	Late[c,f]
S1-34	...	13.20 ± 0.14	1.29	0.86	−0.96	50	...
S2-5[h]	GEN+1.91−0.86	13.32 ± 0.05	2.05	1.89	−0.80	50	Early[g]
S1-68[h]	...	13.38 ± 0.06	1.97	1.89	−0.55	50	...
S2-21	GEN−1.70−1.65	13.47 ± 0.10	2.36	−1.70	−1.65	12	Early[g]
S0-13[h]	GEN+0.59−0.47	13.49 ± 0.04	0.69	0.54	−0.42	50	Late[c,f]
S1-25[h]	GEN+1.69−0.66	13.54 ± 0.05	1.76	1.65	−0.60	50	Late[f]
S2-26	...	13.60 ± 0.13	2.56	0.69	2.47	20	Late[f]
S0-15	E16:W5	13.70 ± 0.07	0.98	−0.93	0.29	48	O9-9.5 V[b]
S0-14	E14:W9	13.72 ± 0.08	0.83	−0.78	−0.27	50	O9.5-B2 V[b]
S1-19	GEN+0.38−1.58	13.82 ± 0.12	1.62	0.36	−1.58	46	Early[g]
S2-2	GEN−0.54+2.00	14.07 ± 0.11	2.12	−0.59	2.03	41	Late[g]
S0-2	E1:S2	14.16 ± 0.08	0.12	−0.07	0.10	33	B0-2 V[j]
S1-8	E18:W11	14.19 ± 0.11	1.08	−0.67	−0.85	49	OB[b]
S1-15	W4	14.21 ± 0.10	1.46	−1.37	0.52	47	Late[g]
S0-6	S10	14.26 ± 0.09	0.39	0.07	−0.38	49	Late[g]
S1-49	...	14.26 ± 0.13	1.66	−1.65	0.15	23	...
S1-13	W12	14.27 ± 0.12	1.42	−1.10	−0.90	46	Early[g]
S2-47	...	14.29 ± 0.08	2.26	2.20	−0.49	48	Early[g]
S0-9	S11	14.31 ± 0.08	0.55	0.14	−0.53	49	Early[g]
S0-12	W6	14.38 ± 0.06	0.68	−0.57	0.37	49	Late[g]
S2-3	W15	14.48 ± 0.09	2.09	−1.54	−1.41	23	Late[g]
S0-4	E10:S8	14.49 ± 0.11	0.37	0.32	−0.19	49	B0-2 V[j]
S0-3	E6:S4	14.50 ± 0.14	0.25	0.22	0.13	19	B0-2 V[j]
S2-75	...	14.52 ± 0.12	2.78	2.65	−0.85	40	...
S2-69	...	14.57 ± 0.14	2.64	−0.91	2.48	13	Early[g]
S3-4	...	14.61 ± 0.20	3.14	3.10	−0.47	20	Early[g]
S0-1	E4:S1	14.67 ± 0.11	0.14	−0.11	−0.09	49	B0-2 V[j]
S2-23	...	14.72 ± 0.13	2.43	1.64	1.80	39	Late[g]
S1-55	...	14.80 ± 0.39	1.69	1.58	0.59	41	...
S1-50	...	14.82 ± 0.37	1.67	1.51	0.72	41	...
S1-52	...	14.83 ± 0.29	1.66	−0.02	1.66	42	...
S1-10	W8	14.88 ± 0.12	1.15	−1.15	−0.04	42	...
S1-2	E17:GEN−0.06−1.01	14.90 ± 0.12	1.00	−0.05	−1.00	45	Early[g]
S1-33	...	15.01 ± 0.10	1.25	−1.24	−0.07	40	...
S1-58	...	15.04 ± 0.35	1.77	−1.48	0.98	37	...
S1-51	...	15.05 ± 0.15	1.66	−1.65	−0.20	39	Early[g]
S2-86	...	15.05 ± 0.23	2.99	2.68	−1.33	24	Early[g]
S3-3	...	15.06 ± 0.33	3.12	3.06	−0.62	19	Early[g]
S2-30	...	15.13 ± 0.19	2.88	2.88	0.00	23	...
S1-18	...	15.14 ± 0.15	1.66	−0.73	1.49	39	Early[g]

TABLE 3—*Continued*

Star ID	Other ID	K[a] (mag)	p (arcsec)	ΔR.A. (arcsec)	ΔDecl. (arcsec)	Nights (days)	Type
S0-5	E9:S9	15.17 ± 0.16	0.36	0.18	−0.31	43	B0-2 V[j]
S0-31	E13	15.20 ± 0.23	0.66	0.49	0.45	40	B V[b]
S2-34	...	15.21 ± 0.22	2.04	1.79	0.98	43	...
S0-26	E8:S5	15.27 ± 0.22	0.39	0.36	0.16	40	B4-9 V[j]
S1-44	...	15.28 ± 0.41	1.61	0.26	1.59	40	...
S3-16	...	15.30 ± 0.20	3.15	3.02	−0.88	14	Late[g]
S2-82	...	15.30 ± 0.29	2.88	2.87	0.08	27	Late[g]
S2-12	...	15.33 ± 0.17	2.07	1.68	1.22	38	Late[g]
S1-32	...	15.33 ± 0.13	1.13	−0.93	−0.64	42	...
S1-39	...	15.35 ± 0.16	1.45	−0.53	−1.35	30	Early[g]
S0-11	E12:S7	15.36 ± 0.13	0.53	0.53	−0.01	40	B V[b]
S0-18	S18	15.36 ± 0.13	0.43	−0.09	−0.42	45	...
S1-35	...	15.36 ± 0.19	1.27	−1.24	−0.25	38	...
S2-63	...	15.39 ± 0.28	2.56	−0.69	2.47	16	Early[g]
S1-54	...	15.41 ± 0.23	1.68	−1.53	0.70	36	...
S1-62	...	15.41 ± 0.31	1.82	0.51	1.74	37	...
S1-53	...	15.44 ± 0.15	1.68	1.68	−0.09	30	...
S2-61	...	15.46 ± 0.17	2.54	2.46	−0.64	38	...
S2-46	...	15.47 ± 0.30	2.18	2.08	−0.64	38	...
S2-73	...	15.50 ± 0.32	2.72	2.21	−1.58	29	...
S1-6	...	15.54 ± 0.13	1.15	−0.91	0.71	34	Early[g]
S1-48	...	15.54 ± 0.23	1.62	−0.60	−1.50	22	...
S0-7	E11:S6	15.55 ± 0.27	0.45	0.44	0.11	35	B V[b]
S0-19	E5	15.56 ± 0.19	0.19	−0.09	0.17	28	B4-9 V[j]
S1-64	...	15.57 ± 0.36	1.91	0.60	1.81	34	...
S2-80	...	15.57 ± 0.27	2.86	2.22	1.80	20	Early[g]
S2-40	...	15.58 ± 0.18	2.15	1.68	1.34	35	Early[g]
S2-42	...	15.61 ± 0.28	2.11	0.41	2.07	26	...
S1-27	...	15.62 ± 0.27	1.09	−1.07	0.24	39	...
S1-26	...	15.62 ± 0.13	1.02	−0.95	0.38	40	...
S1-37	...	15.63 ± 0.16	1.42	−1.34	0.47	36	...
S1-47	...	15.67 ± 0.23	1.63	−1.57	0.45	34	...
S0-16	E2	15.68 ± 0.19	0.08	0.05	0.06	18	B4-9 V[j]
S1-59	...	15.70 ± 0.25	1.86	0.01	1.86	27	...
S1-31	GEN−0.91+0.44	15.70 ± 0.18	1.14	−0.99	0.57	31	...
S0-29	...	15.72 ± 0.50	0.54	0.25	−0.48	21	...
S2-83	...	15.74 ± 0.19	2.94	2.87	−0.63	16	...
S0-27	...	15.74 ± 0.18	0.54	0.13	0.52	32	...
S1-36	...	15.75 ± 0.27	1.36	−0.67	−1.18	30	...
S2-37	...	15.77 ± 0.31	2.11	0.04	2.11	29	...
S0-8	E7	15.79 ± 0.14	0.47	−0.32	0.34	29	B4-9 V[j]
S1-7	...	15.81 ± 0.14	1.12	−1.00	−0.50	34	...
S1-65	...	15.82 ± 0.15	1.93	1.43	1.29	31	Early[g]
S0-28	S19	15.85 ± 0.18	0.61	−0.18	−0.58	30	...
S2-64	...	15.85 ± 0.59	2.56	2.54	0.31	16	...
S0-36	...	15.85 ± 0.28	1.03	−0.60	−0.84	29	...
S0-20	E3	15.86 ± 0.20	0.21	−0.18	−0.10	33	B4-9 V[j]
S1-40	...	15.95 ± 0.23	1.50	−1.36	−0.64	26	...
S1-61	...	15.99 ± 0.38	1.76	−1.43	−1.03	21	...
S2-52	...	16.02 ± 0.20	2.37	2.37	−0.07	21	...
S1-42	...	16.13 ± 0.22	1.60	0.94	1.29	19	...

NOTE.—All observations are speckle K-band ($\lambda_0 = 2.2$ μm, $\Delta\lambda = 0.4$ μm) images.

[a] The magnitudes are Q_j corrected using seven bright nonvariable stars, and the uncertainties do not include the 5% calibration uncertainties. Comparison to other sources requires adding them in quadrature.

[b] Spectroscopic identification by Paumard et al. (2006).

[c] Identified as nonvariable by Ott et al. (1999).

[d] This is our main calibration star and is included in this table only for completeness.

[e] Spectroscopic identification by Figer et al. (2003).

[f] Spectroscopic identification by Ott (2003). We denote sources with clear CO or He lines as Early and Late, respectively.

[g] Identification based on the interpretation by Genzel et al. (2003) of m(CO) index of Ott (2003), where Genzel et al. (2003) identify stars with $m(\mathrm{CO}) \geq 0.04$ as late-type stars and stars with $m(\mathrm{CO}) < 0.04$ as early-type stars.

[h] The seven least variable bright stars detected in all images used for scaling of the photometry in order to reduce the fluctuations induced by measurement errors on IRS 16C (see § 3.1).

[i] Identified as possibly variable by Ott et al. (1999).

[j] Spectroscopic identification by Eisenhauer et al. (2005).

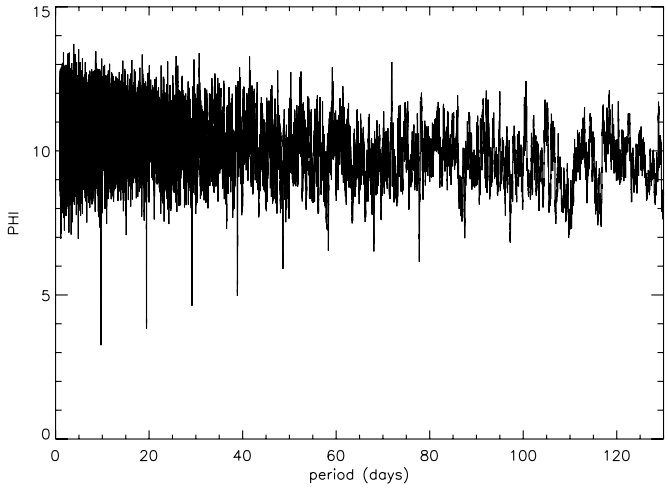

FIG. 6.—Determination of IRS 16SW's period using Dworetsky's string length method (Dworetsky 1983). "Phi" is the string length where shorter lengths, and therefore smaller values of Phi indicate a periodic signal. Note that the other harmonics are also found at multiples of the original period.

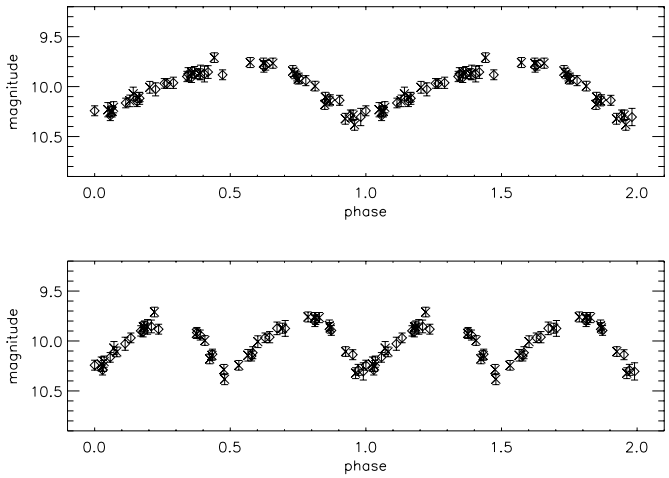

FIG. 7.—Phased light curve of IRS 16SW at its period of 9.724 (*top*) and 19.448 days (*bottom*). The points are plotted twice for clarity. Both phased diagrams show a rise time that is ~1.6 times longer than the fall time. The similarity of the first half of the data set (1995–2000; *diamonds*) to the second half (2001–2005; *crosses*) shows that the asymmetry has been constant over the past 10 yr. This effect could be produced by tidal deformation of two equal-mass stars in an eclipsing binary star system.

the Galactic center. Those authors give an upper limit of possible variable stars of approximately 50% of their 218 sources with $m_K < 13$ mag over $18'' \times 18''$. While this variable star frequency is higher than our reported value (and consistent), a comparison limited to the stars in common leads to a number of discrepancies. In the overlap sample of 33 stars, Ott et al. find two of the stars to be variable (IRS 16SW, S1-3), while our sample has six (IRS 16SW, IRS 16NW, IRS 29N, S2-11, S2-4, and S1-21), and only IRS 16SW is in common. There are a number of differences between these two studies, including the data analysis approach used (PSF fitting vs. aperture photometry), the time baseline (10 vs. 5 yr), and the angular resolution ($0.05''$ vs. $0.13''$). Since our study covers twice the time baseline, we can pick out variations on longer timescales, which helps explain our additional variables. Also, the high stellar crowding makes the area we observe the most uncertain region for the lower resolution Ott et al. study. Only one star, S1-3, in our nonvariable sample is identified as variable by Ott et al., and it is very close to their threshold for variability.

3.2.2. *Variability Characterization and Periodicity Search*

We attempt to characterize the minimum timescale for variation by searching for daily and monthly variability using K-S tests similar to the test for variability in § 3.2.1, where we adopt as our model a nonvariable light curve with Gaussian-distributed uncertainties. For the daily variations, we group the consecutive nights in pairs and examine the distribution of the pairs in sets i for each star of $X_i = [\mathrm{flux}_j - \mathrm{flux}_k/(\sigma^2_{\mathrm{flux}_j} + \sigma^2_{\mathrm{flux}_k})^{1/2}]$, where flux_j and flux_k are the fluxes of stars in images of consecutive epochs j and k, respectively, and σ_{flux_j} and σ_{flux_k} are the corresponding uncertainties. For the monthly variation, all measurements made within days of each other are averaged together, and the pairs separated by 1 month are examined with the same K-S test. The only stars showing daily variability in excess of 3 σ is IRS 16SW, and the stars showing monthly variations are IRS 16SW and S2-36.

The light curves of the variable stars are searched for periodicities using three different methods. First, the Lomb and Scargle periodogram technique (Lomb 1976; Scargle 1982; Press et al. 1992), which fits Fourier components to the data points, is applied and is expected to yield a larger power spectral density at intrinsic harmonics of a data set in which there is a periodic signal. Second, Dworetsky's (1983) string length method, a variant of the Lafler-Kinman method (1965), phases the data for every possible period and then sums over the total separation between points in phase space, with the best period and its aliases corresponding to the smallest lengths. Third, Stetson's (1996) string length technique is similar to Dworetsky's, but also weights these lengths by their uncertainties and how close in phase the points are. Our criterion for considering a star periodic is that it show similar periods from all three techniques. The periodicity search shows only one periodic star: IRS 16SW. We find a photometric period of 9.724 ± 0.001 days, which is consistent with Ott et al. (1999), DePoy et al. (2004), and the reanalysis of the Ott et al. data in Martins et al. (2006). Figure 6 shows the determination of IRS 16SW's period using Dworetsky's (1983) string length algorithm, showing the 9.724 day period and its other harmonics at multiples of its period. The top panel in Figure 7 shows the phased light curve of IRS 16SW at 9.724 days and depicts a clearly periodic signal with an amplitude of ~0.55 mag. The phased light curve of IRS 16SW is asymmetric (see Fig. 7) with a rise time that is ~1.6 times longer than the fall time.

4. DISCUSSION

The 16 variable stars identified in this study cover a wide variety of different types of stars, as we only limited our search by location and brightness. As Figure 14 shows, based on the K magnitudes alone, this sample is expected to contain early-type (O and B) main-sequence stars, late-type (K and M) giant stars, and most types of supergiants. Fortunately, all but two of the variable stars have spectral classifications (see col. [10] in Table 2). While nine of the variable stars are securely identified from spectroscopic work (Paumard et al. 2006; Eisenhauer et al. 2005; Figer et al. 2003; Ott 2003), an additional five stars are classified on the basis of narrowband photometry of CO absorption (Ott 2003; Genzel et al. 2003). In summary, four stars are LBV candidates (IRS 16SW, 16NW, 16NE, and 16C; see § 4.1), one is a WC9 (IRS 29N; see § 4.2), four are OB supergiants (S2-4, S1-12, S2-7, and IRS 16CC; see § 4.3), one is an O giant (S1-21), five more are classified as some sort of early-type star from narrowband filter photometric measurements (S1-1, S2-36, S0-32, S2-58, and S1-45), and one is classified as a late-type star from narrowband filter photometric measurements (S2-11; see

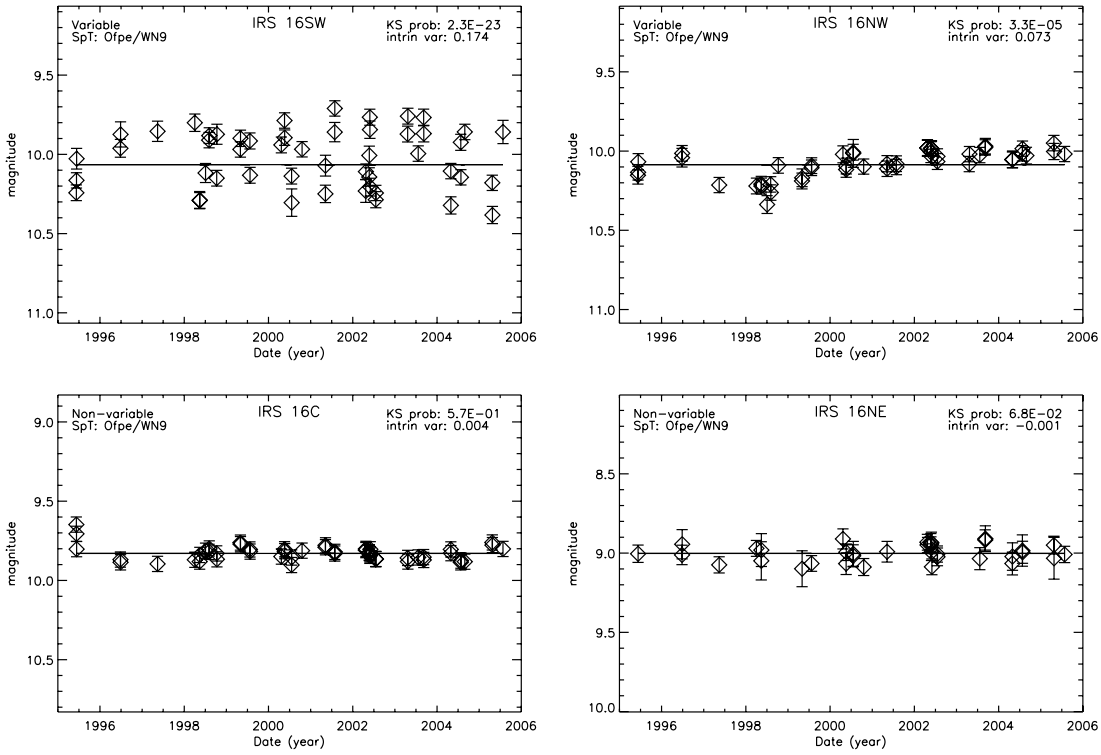

FIG. 8.—Light curves of the four stars in our sample that are classified as candidate LBVs (IRS 16SW, 16NW, 16NE, and 16C). The top two panels denote the two variable stars, while the bottom two panels are nonvariable stars. The given intrinsic variance is in magnitudes.

§ 4.3). The variability of stars in each spectral classification is discussed in turn below, along with a discussion of the possibility of external agents causing variability.

4.1. *Ofpe/WN9 Stars*

4.1.1. *Luminous Blue Variable Candidates*

Four stars in our sample are Ofpe/WN9 stars and have been previously classified as candidate LBVs (IRS 16NE, 16C, 16SW, and 16NW) based on their bright luminosity, their narrow emission lines, and their proximity and similarity to IRS 34W (Clark et al. 2005; Paumard et al. 2004a; Trippe et al. 2006).[5] In our observations, both IRS 16NE and 16C are nonvariable over a 10 yr time frame to within our uncertainties. The other two LBV candidates (IRS 16NW and 16SW) show variability, but not the characteristic LBV eruptions, which in the context of this study are the $\Delta M_v \simeq 1$–2 mag events occurring every 10–40 yr and lasting as long as several years (Humphreys & Davidson 1994). IRS 16SW has periodic variability that is explained by an eclipsing binary system (see § 4.1.2 below), and IRS 16NW has an overall flat light curve with a decrease in brightness ($\Delta m_K \simeq 0.2$) mag between 1997 and 1999 (see Fig. 8). The apparent dimming of IRS 16NW can be explained by ejected circumstellar material obscuring the star, with an amplitude that is smaller than is characteristic of a typical LBV. These variations do not require it to be an LBV, just that it has strong stochastic winds. While none of these stars show the classic characteristics of LBVs, our time baseline is too short to rule them out as LBVs, as they may be in a quiescent phase. Nonetheless, our observations do not demand the complication of multiple recent star formation events that would be suggested with the presence of both LBVs and W-R stars.

4.1.2. *Asymmetric Periodic Light Variations in IRS 16SW: Tidal Deformation?*

The periodic variation in IRS 16SW has recently been attributed to either an equal-mass contact eclipsing binary or a massive pulsating star (Ott et al. 1999; DePoy et al. 2004; Martins et al. 2006), although the measurement of a spectroscopic radial velocity period by Martins et al. (2006) strongly suggests it is an eclipsing binary star system. Also, a reanalysis of the data suggesting a pulsating star now agrees with IRS 16SW probably being an eclipsing binary (Peeples et al. 2007). The asymmetries that we observe in the phased light curve of IRS 16SW are difficult to explain in the context of an eclipsing binary star system. Figure 7 shows the properly phased light curve (19.448 ± 0.002 days), in which asymmetries in its rise and fall times are still readily detected. The asymmetry is remarkably similar for both halves of the phased light curve. While this was not detected in earlier photometric studies,[6] our study is likely more sensitive to small photometric variations due to our higher angular resolution (see § 3.2.1). The observed asymmetry has been sustained over 10 yr; if the asymmetry has been changing over time, it would show up as a dispersion in the vertical placements of the points in the phase diagram that is much larger than what we observe. In Figure 7 we explicitly show that the asymmetries are the same during the first half and second half of the data set, and we see no period drifts, with the period of the first half and second

[5] The classification of IRS 34W as an LBV is based on its bright luminosity and narrow emission lines, along with a multiyear obscuration event (Paumard et al. 2004b; Trippe et al. 2006). However, more recent studies have cast doubt on IRS 34W's categorization as an LBV, since it lacks spectroscopic variability and since the eruption event responsible for the obscuration event was not observed (Trippe et al. 2006).

[6] Our light curve is similar to the light curve presented by Ott et al. (1999), although the asymmetry was not explicitly reported and the reanalysis of the data by Martins et al. (2006) does not show the asymmetry.

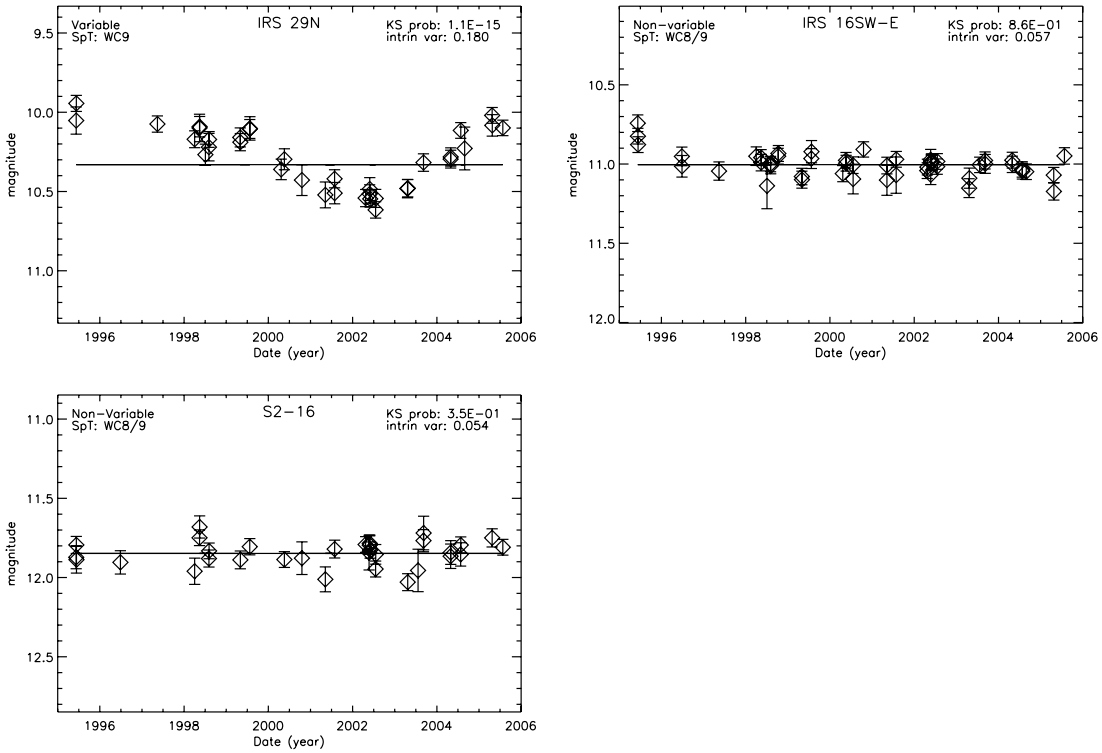

FIG. 9.—Light curves of W-R stars of type WC in our sample. The top left panel is the variable star IRS 29N, which is probably a wind-colliding binary, while the other two are nonvariable stars. The given intrinsic variance is expressed in magnitudes.

half not differing at the 3 σ confidence level. Magnetic hot spots can explain light-curve asymmetries (Djurašević et al. 2000; Cohen et al. 2004); however, they cannot maintain this asymmetry over long periods of time. Furthermore, the similarity in the asymmetry between the first and second half would require the spots to be the same on both stars. Likewise, heating in the contact region of the binary or any third light in this region produces a light curve that is a mirror reflection between the first and second half (see Moffat et al. 2004) and is therefore inconsistent with our observations. Other heating mechanisms such as irradiation effects are unlikely to be the cause of the asymmetry, as they barely change the light curve (Bauer 2005). Given that this is suspected to be a contact binary, we suggest that the asymmetric light curve may be due to tidal deformations caused by the proximity of the stars in asynchronous orbits. Since these two stars are equal in mass ($\sim$50 $M_{\odot}$), equal in radius (66 $R_{\odot}$), and appear to be in contact (Martins et al. 2006), they fall within the tidal radius of $\sim$163 $R_{\odot}$ and are likely tidally deformed. In order to produce the asymmetric light curve, the rotation of the stars needs to be asynchronous with their orbital periods so that the rotational inertia of the stars prevents their tidal bulges from being aligned with the line joining the stars' centers of mass. Two stars in such close contact will eventually synchronize their orbital period with their rotation period. The synchronization timescale of stars with convective cores and radiative envelopes is longer than for stars with convective envelopes, albeit more difficult to calculate (Zahn 1977). We therefore calculate the convective envelope synchronization time as a minimum time for synchronization based on formalism developed by Zahn (1977) and find a minimum age of $\sim 6 \times 10^8$ yr. This timescale is far larger than the lifetime of stars as massive as IRS 16SW, and asynchronous orbits are therefore acceptable. The equality of the two halves of the light curve implies that the rotation rate of the two stars is very similar. Since these two stars are identical in every other respect, this equality is not surprising. It is therefore possible that the asymmetric light curve is due to tidal deformations.

4.1.3. *Eclipsing Binary Fraction*

Stars close to the Galactic center are expected to have a higher fraction of ellipsoidal and eclipsing variable binaries than the stars in the solar neighborhood. However, IRS 16SW is the only eclipsing binary star detected in our sample. The stars' orbits may be smaller due to hardening by encounters with other stars producing tightly bound binaries, such that eclipses would be more likely. In addition, collisions and tidal capture produce binaries, making ellipsoidal variations or eclipses more probable (Tamura et al. 1996). Of the 164 Galactic O stars in clusters or associations in the sample by Mason et al. (1998) 50 are confirmed as spectroscopic binaries, 40 are unconfirmed spectroscopic binaries, four are confirmed eclipsing variables, and 14 are either ellipsoidal or eclipsing binaries. This yields local rates of eclipsing O star binaries between 2% and 11%. Our sample contains 11 spectroscopically confirmed O stars, four Ofpe/WN9 stars, and possibly more unconfirmed. If the Galactic center fraction of eclipsing binaries is similar to the cluster results, we would expect of order one eclipsing binary. Our detection of one eclipsing variable star suggests that the frequency of eclipsing binaries is not significantly increased at the Galactic center over the local neighborhood.

4.2. *Late-type WC Wolf-Rayet Stars: Variations Associated with a Wind Colliding Binary*

Three stars in our sample are spectroscopically identified as WC stars (IRS 29N, IRS 16SW-E, and S2-16) (Paumard et al. 2006), and all three are dust producers, as evidenced by their red colors ($K-L \sim 3$; Blum et al. 1996a; S. A. Wright et al. 2007, in preparation). In this study, only IRS 29N is variable (see Fig. 9). IRS 29N's intensity shows a gradual drop and then rise in

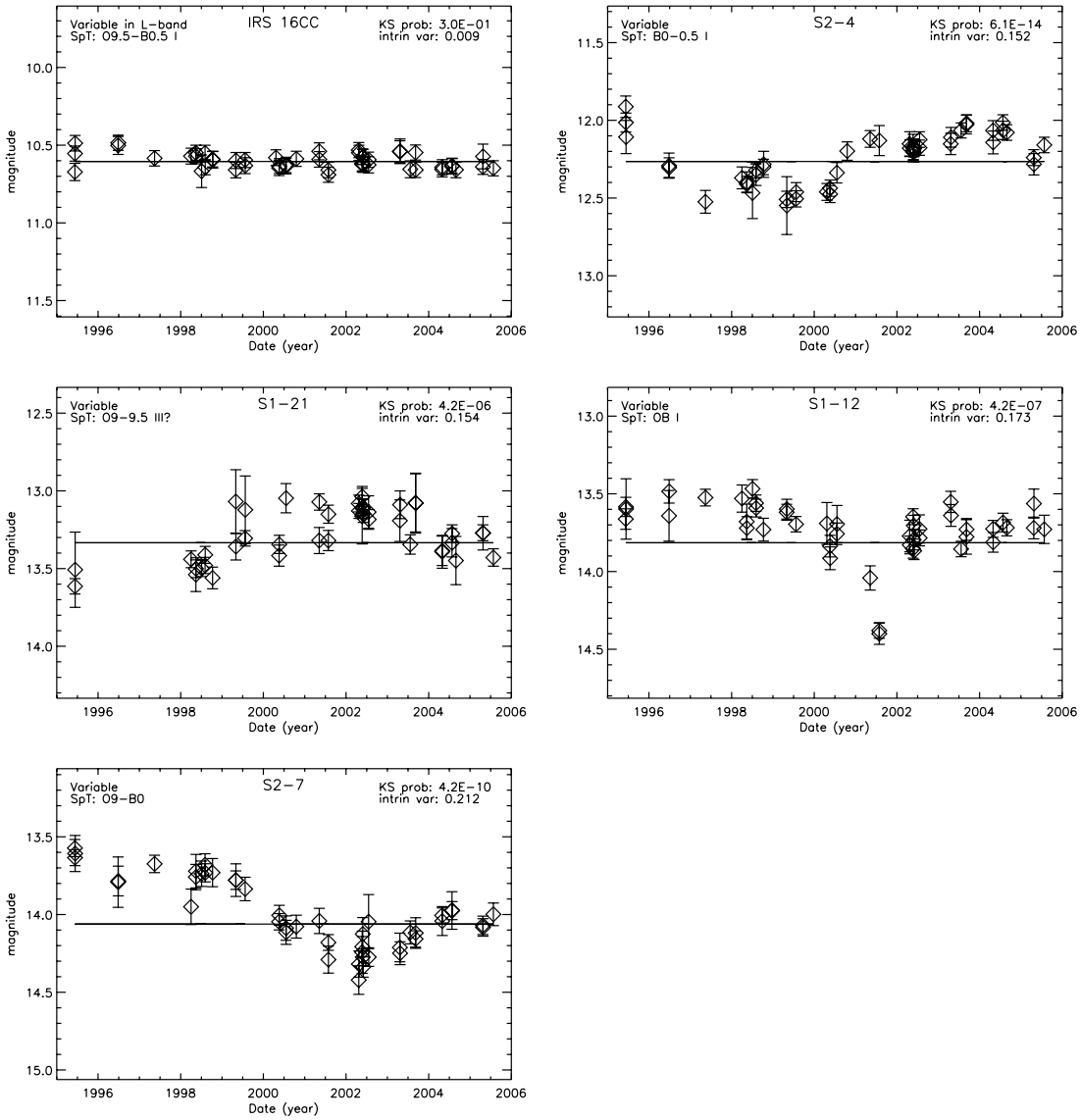

FIG. 10.—Light curves of variable OB stars in our sample. IRS 16CC is not variable in K band, but shows variability at L (see § 3.1). We propose that S2-4 and S1-12 are variable due to ejection of circumstellar material obscuring the stars, while S2-7 is probably a Be star with the formation of an equatorial disk obscuring the star. The given intrinsic variance is expressed in magnitudes.

brightness of $\Delta m_K \simeq 0.7$ mag over a timescale of ≈5 yr. Its light curve is similar to the variations seen in WC stars elsewhere in the Galaxy (e.g., compilation by van der Hucht et al. 2001); these sources are thought to be variable due to periodic or episodic dust production in the wind collision zone of long-period eccentric binary star systems (1000 days $< P <$ 10,000 days) during periastron passage. When the dust forms, the star exhibits a rising infrared flux followed by fading emission when dust formation stops and dust grains are dispersed by stellar winds (Moffat et al. 1987; White & Becker 1995; Veen et al. 1998; Williams & van der Hucht 1992, 2000). Currently, only seven WC stars have been observed to produce dust episodically, all of which are confirmed or suspected massive binaries with elliptical orbits (van der Hucht 2001; Williams et al. 2005; Lefèvre et al. 2005). Two of these are known to exhibit pinwheel nebulae, a tell-tale sign of wind-colliding binaries (Tuthill et al. 1999; Monnier et al. 1999). The timescales and magnitude of the photometric variability of IRS 29N is consistent with it being a wind-colliding binary; we therefore conclude that IRS 29N is likely to be a wind-colliding binary.

4.3. *Comments on Other Stars*

Our sample includes at least 10 other variable young massive stars in addition to those discussed in §§ 4.1 and 4.2. Five are spectroscopically identified OB stars (IRS 16CC,[7] S2-4, S1-21, S1-12, and S2-7; see Fig. 10) (Paumard et al. 2006), and five are early-type stars classified as on the basis of narrowband filter photometric measurements (S1-1, S2-36, S0-32, S2-58, and S1-45; see Fig. 11) (Genzel et al. 2003; Ott 2003). The majority of these variables are likely associated with mass loss, although interstellar extinction could also play a role, as discussed below. In particular, the two K-band variable OB supergiants each show a dip (0.3–0.9 mag) in their brightness that lasts for 1–6 yr. OB supergiants have stochastic winds with high mass-loss rates [$(0.2–20) \times 10^{-6}\ M_\odot\ \mathrm{yr}^{-1}$; Massey 2003]; it is therefore likely

[7] IRS 16CC is not identified as variable in this survey, although reported differences in L-band magnitudes from previous studies suggest it is variable (Depoy & Sharp 1991; Simons & Becklin 1996; Blum et al. 1996a; S. A. Wright et al. 2007, in preparation) (see § 3.1).

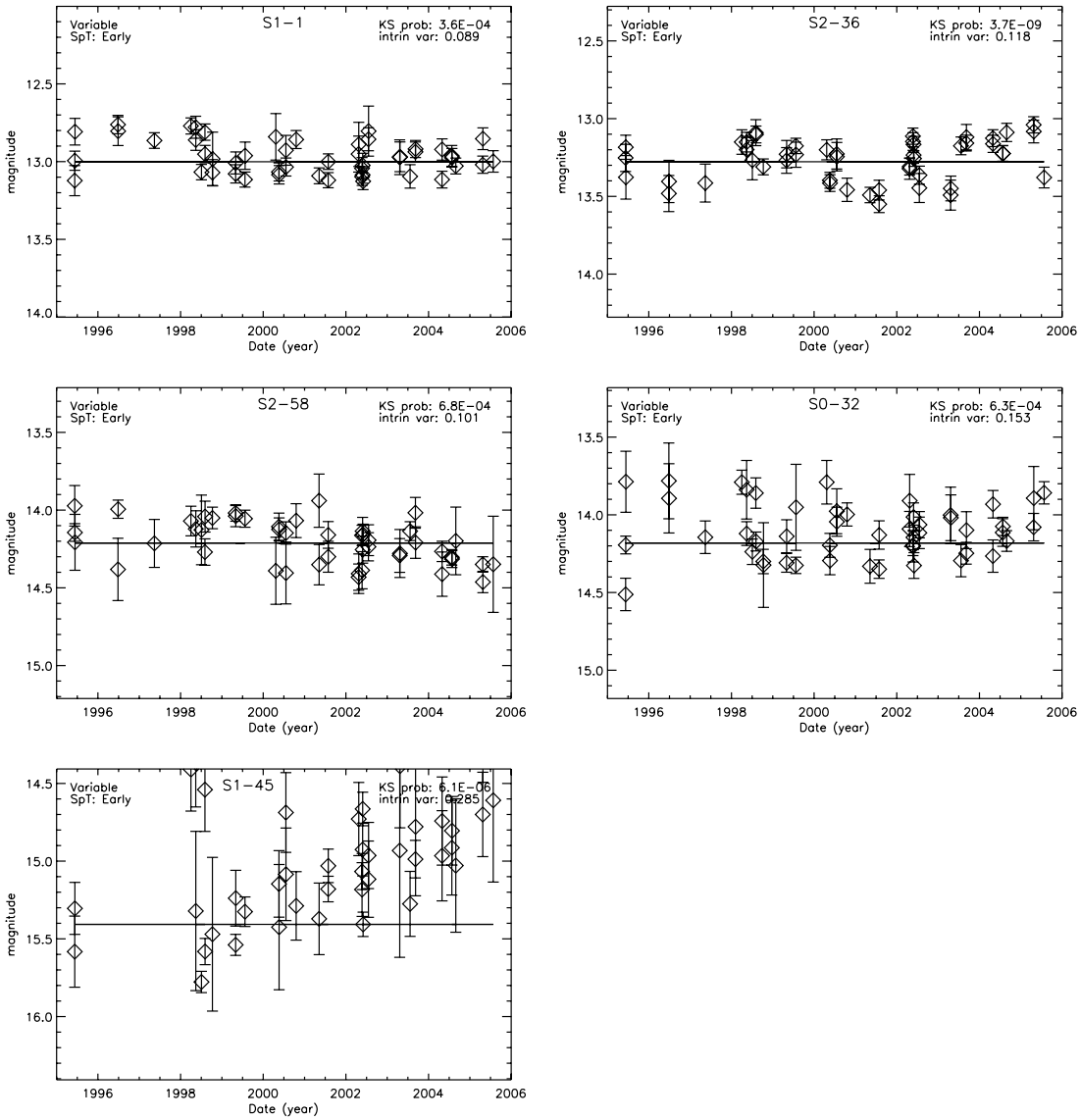

FIG. 11.— Light curves of early-type variable stars in our sample; S2-36 is variable on a monthly basis, and its variation is therefore probably intrinsic. The variations in S1-45 and S2-58 may be due to obscuration by high-density streamers. The given intrinsic variance is expressed in magnitudes.

the large variations seen are due to ejection of circumstellar material. Another example of an OB star with variations potentially due to mass loss is S2-7, which is either luminosity class III or V based on its assumed distance. S2-7 shows a decrease in luminosity between 2000 and 2005 with $\Delta m_K \simeq 0.5$–1.0 mag. This is reminiscent of Be stars, which sometimes show fading events due to the formation of an equatorial disk on timescales of several years (Mennickent et al. 1994; Pavlovski et al. 1997; Percy & Bakos 2001). The remaining young variable stars in our sample have variations that are more difficult to characterize, although S2-36 seems to have significant variations on monthly timescales (see § 3.2.2). Nonetheless, it is likely that mass loss also plays a central role in generating the observed variations.

4.4. *Interstellar Material*

4.4.1. *Apparent Variations Caused by Stellar Motion through the Line-of-Sight Extinction*

Periods of reduced luminosity in stars can also be due to external effects such as obscuration by foreground interstellar matter. The central parsec has several gas patches that are a few arcseconds wide and that can cause local extinction enhancements of $\sim$1 mag in K band (Paumard et al. 2004b). As our FOV is only $5'' \times 5''$, these patches would cover a sizable region, and many neighboring stars would show similar variations. Interstellar material closer to Earth in the line of sight is unlikely, as its proximity would make the clouds even larger in projection (Trippe et al. 2006). Since neighboring stars do not experience similar effects of obscuration, the large-scale structure in the interstellar medium is unlikely to be the cause.

In some cases it is possible that the variable obscuration is caused by the relative motion of the foreground high-density streamers and the background stars, such as are observed in the L band associated with the northern arm (Clénet et al. 2004; Ghez et al. 2005b; Mužič et al. 2006). In this area we see unresolved streamers that are small in projected width ($<$80 mas). These streamers may be due to shocks heating the neighboring dust with the streamers tracing thin shells of compressed gas from one or several shocks (Clénet et al. 2004). These streamers may cause dips in our light curves due to small-scale structure obscuration

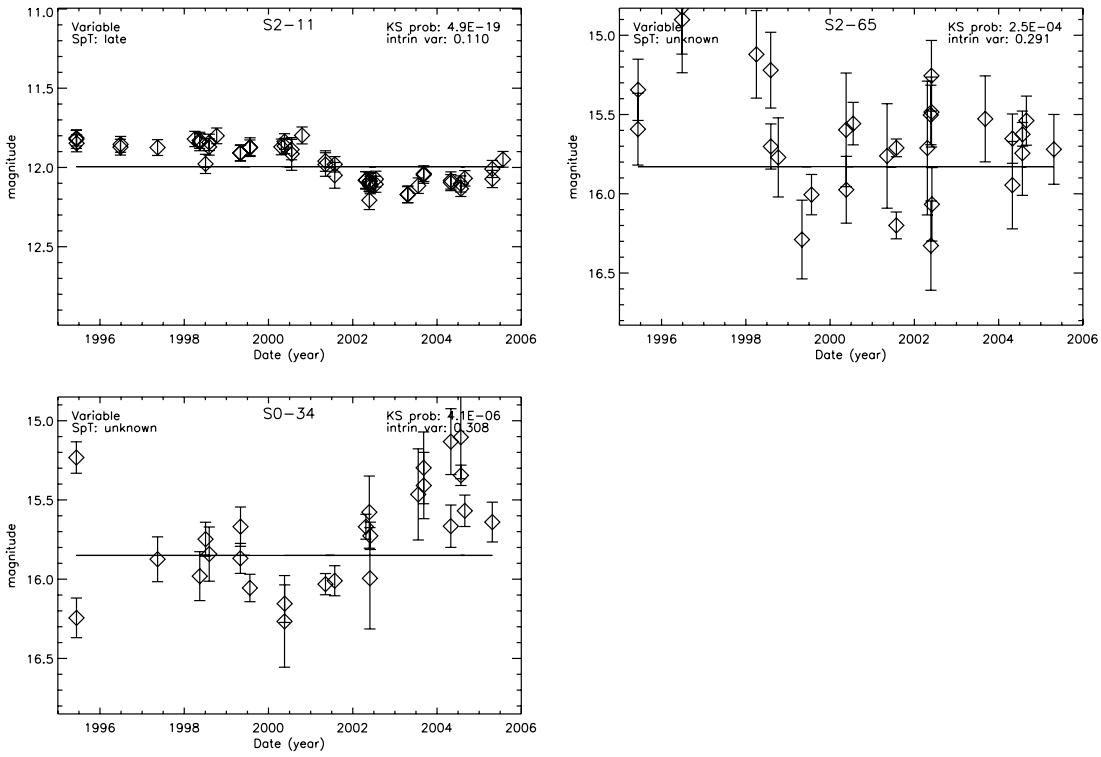

FIG. 12.—Light curves of a late-type star, and two unknown type stars in our sample. The late-type star, S2-11, is probably an AGB star of spectral type M3-5 III, while we are unable to classify the two stars of unknown spectral type. The given intrinsic variance is expressed in magnitudes.

in the line of sight. This causes photometric variability due to the relative lateral motion between the absorbing feature and the star. The projected implied width of the small-scale structure is approximately ~10–40 mas, assuming a projected stellar velocity of ~5 mas yr^{-1}, which is typical of stars at projected distances of ~2″ from Sgr A*. The three stars whose variability is most likely ascribable to these thin high-density streamers are S2-11, S1-45, and S2-58. The most clear case is the late-type star S2-11 (Ott 2003), which shows an interval of reduced luminosity between 2001 and 2005 with $\Delta m_K \simeq 0.3$ mag and is otherwise constant over our time frame (see Fig. 12). Using a Galactic center distance of $r = 8.0$ kpc (Reid 1993) and an extinction $A_K = 3.3$ mag (Blum et al. 1996a), we determine its spectral type based on luminosity and late-type classification as M3-5 III. Stars with spectral type M5 and luminosity class III are generally classified as asymptotic giant branch stars (AGB), but the variations observed are not typical of AGB stars, which have periods between 0.5–1.5 yr (Habing 1996). This star is likely obscured by dust given its red color ($K-L \sim 2$; S. A. Wright et al. 2007, in preparation). It is located in the middle of the northern arm (see Fig. 15), and its reduced luminosity is likely due to a high-density streamer in the line of sight. The two other stars whose variability can probably be attributed to high-density streamers have long-term variations over 10 yr; S1-45 appears to brighten by $\Delta m_K \simeq 0.5$–1.0 mag, and S2-58 appears to dim by $\Delta m_K \simeq 0.2$ mag (see Fig. 11). It is also possible that the dips in the light curves of stars speculated to be variable due to high stellar winds such as S2-4, S1-12, S2-7, and S2-36 are actually variable due to obscuration in the line of sight. Measurements at multiple wavelengths throughout future variations would help to establish the role of variable extinction in the observed K-band variations. Furthermore, foreground material would be polarized due to the magnetic fields at the Galactic center, and therefore polarization variations of stars would provide a test of the hypothesis that the relative motion of streamers and stars are responsible for stellar intensity variations.

4.4.2. *Variability of Stars near Closest Approach*

We detect no variability in the seven central arcsecond sources that have known three-dimensional orbits (S0-1, S0-2, S0-4, S0-5, S0-16, S0-19, and S0-20) (see Fig. 13). The three fainter stars (S0-16, S0-19, and S0-20) have missing measurements that are due to insufficient image sensitivity, although they are detected in higher S/N images made from multiple nights of data (Ghez et al. 2005a). The photometry of these stars constrains the properties of a cold, geometrically thin inactive accretion disk around Sgr A*, since in the presence of such a disk we would expect to see nearby stars significantly flaring in the NIR as they passed through and interacted with the disk, and eclipsed at other times. When a nearby star approaches such a disk we would see enhanced NIR flux from reprocessed UV and optical starlight incident on the disk (which we call a flare). Also, we would expect the disk to eclipse the star, reducing the flux from the star in varying amounts depending on the properties of the disk. The timescales vary based on the geometry of the disk but are of order a year and months for the eclipses and flares, respectively (Nayakshin & Sunyaev 2003; Cuadra et al. 2003). An optically thin disk may not fully eclipse stars, and gaps in our observations would allow different geometries of the disk to account for any one star not showing eclipses or flares, as was calculated for S0-2 (Cuadra et al. 2003). However, with the ensemble of stars that we have monitored, the effects of a disk with any orientation should be evident. We constrain the NIR optical depth to be $\lesssim 0.1$. If we assume the NIR standard interstellar dust opacity at 2.2 μm where the dust extinction is approximately $\sim 5 \times 10^{-22}$ cm^2 per hydrogen atom (see Fig. 2 in Voshchinnikov 2002), we find the column

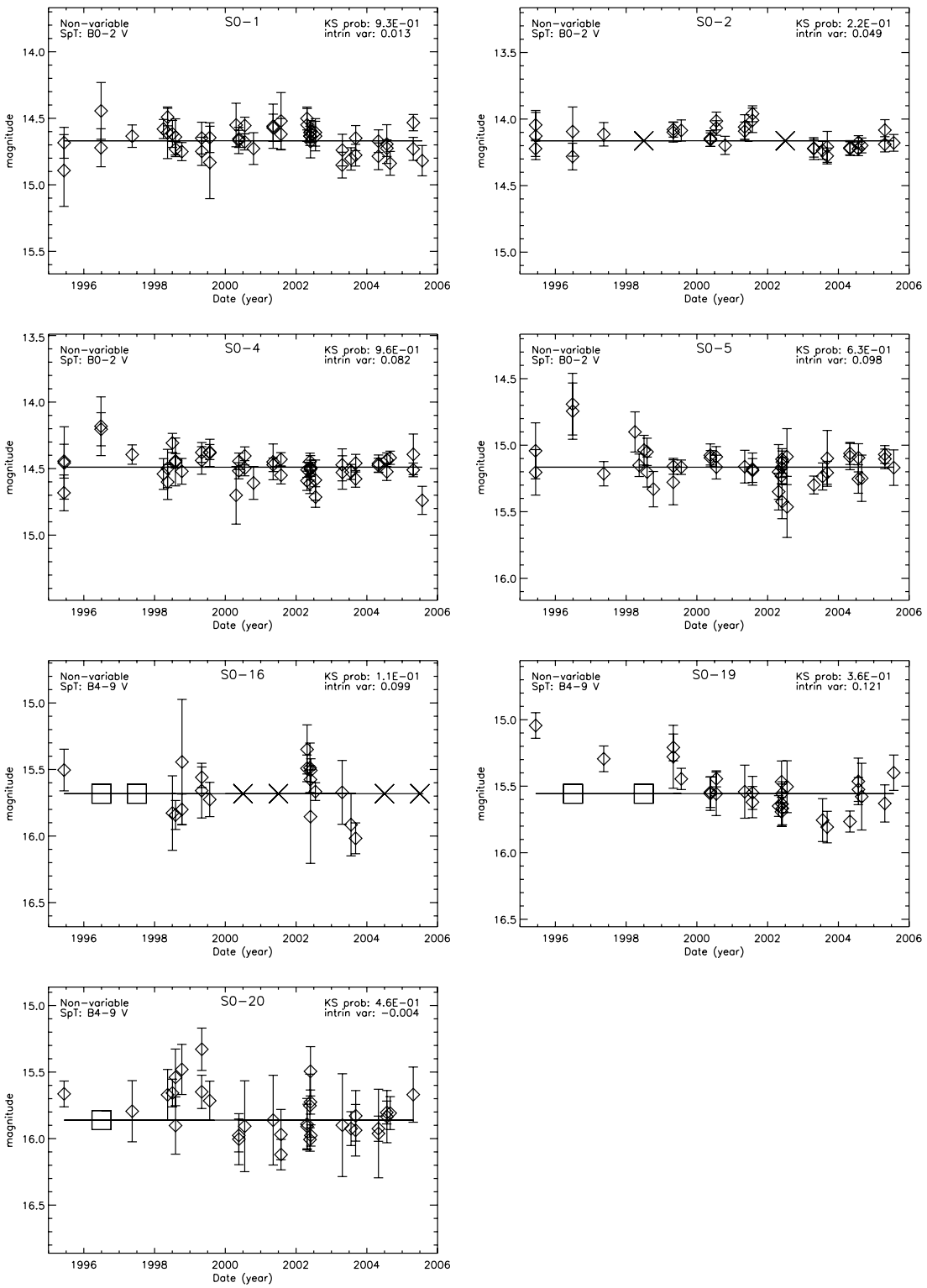

FIG. 13.—Light curves of seven central arcsecond sources that have known three-dimensional orbits. The crosses mark observations that are rejected due to confusion with other sources, and the boxes are areas where the nightly images have missing measurements due to insufficient image sensitivity and correspond to detections in monthly averaged images. None of these stars are variable, which is evidence against the presence of a dusty disk around Sgr A*. The given intrinsic variance is expressed in magnitudes.

density of the disk to be $\sim 2 \times 10^{20}$ cm^{-2}. However, dust grains may be larger in size or nonexistent in the disk (Cuadra et al. 2003; Nayakshin et al. 2004), and such constraints should therefore be approached cautiously. Regardless, the lack of observed flares or eclipses in the seven central arcsecond sources that have known three-dimensional orbits puts such severe constrains on the density and size of any possible disk around Sgr A* that such a disk is unlikely to exist.

5. SUMMARY

We use 10 years of diffraction-limited *K*-band speckle data to determine the photometric stellar variability in the central

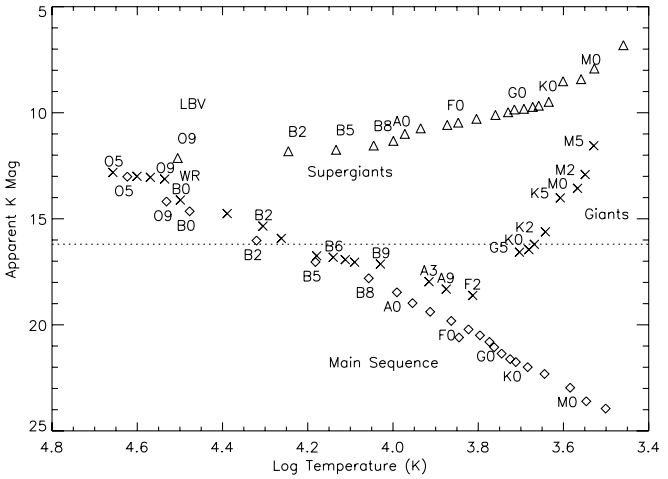

FIG. 14.—Apparent K magnitudes vs. spectral type assuming a distance of $r = 8.0$ kpc (Reid 1993) and an extinction $A_K = 3.3$ mag (Blum et al. 1996a) based on compilations of data from Cox (2000) where available, and by de Jager & Nieuwenhuijzen (1987), Wegner (1994, 2006), Vacca et al. (1996), Grenier et al. (1985), Blackwell & Lynas-Gray (1994), and Theodossiou & Danezis (1991) for giants of type O–F. The dotted line is the magnitude limit of this sample, and the locations of W-R and LBV stars are highly variable; average locations are marked for reference only. The triangles represent supergiant stars, the crosses represent giant stars, and the diamonds represent main-sequence stars.

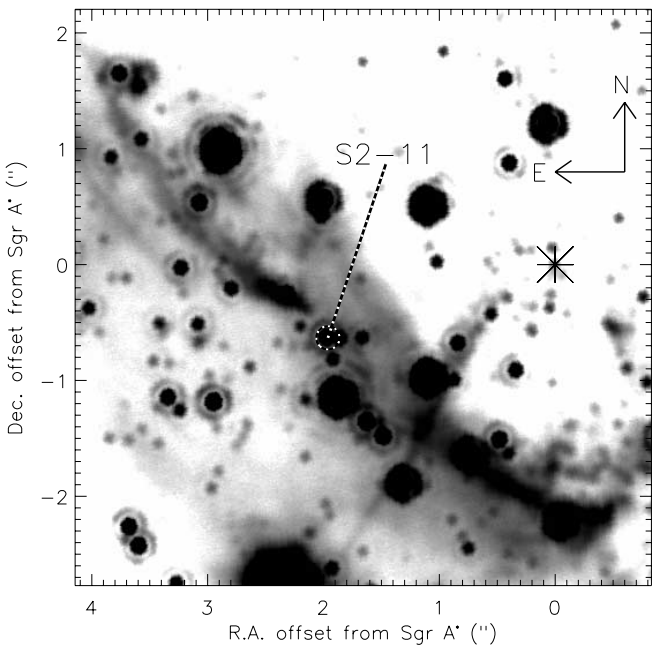

FIG. 15.—Identification of the source S2-11 from this study overlaid on a $5'' \times 5''$ region of an LGS L''-band ($\lambda_0 = 3.8$ μm) image from A. M. Ghez et al. (2007, in preparation) taken on 2005 June 30. The star S2-11 is situated in the middle of the northern arm, and it is therefore likely that the interval of reduced luminosity is due to the stellar motion through a high-density streamer in the line of sight. The location of Sgr A* is marked with an asterisk.

$5'' \times 5''$ of our Galaxy. Within this study's limiting magnitude of $m_K < 16$ mag, we find 15 K-band variable stars out of 131 well-sampled stars. Among 46 stars brighter than $m_K < 14$ mag with uniform photometric uncertainties, there are 10 variable stars, suggesting a minimum variable star frequency of 23%. We find one periodic star, IRS 16SW, with a period of $P = 19.448 \pm 0.002$ days, in agreement with Ott et al. (1999), DePoy et al. (2004), and Martins et al. (2006). Our data are consistent with an eclipsing binary and show a rise time that is $\sim$1.6 times longer than the fall time, and we suggest that the asymmetric light curve results from tidal deformations of the two stars in the presence of asynchronous rotation. We expect to see of order one eclipsing binary in our sample for conditions similar to the rest of the Galaxy, suggesting that the frequency of eclipsing binaries is not significantly increased at the Galactic center over the local neighborhood. We identify IRS 29N as a wind colliding binary based on its light curve and spectral classification. This rare object warrants further investigation to confirm its binary nature. None of the IRS 16 stars show the classic eruptive events of LBVs, although our time baseline is too short to rule them out as LBVs. Among the remaining variable early-type stars in our sample, three exhibit large variations on timescales of a year, which are either due to obscuration from mass-loss events or from line-of-sight extinction variations. Three more stars in our sample exhibit long-term variations of $\sim$5–10 yr probably due to line-of-sight extinction variations due to high-density streamers. Seven stars in the central arcsecond do not show photometric variations indicative of a cold, geometrically thin inactive accretion disk, which puts such severe constraints on the density and size of any possible disk around Sgr A* that such a disk is unlikely to exist.

The authors thank Eric Becklin, Jill Naiman, and Andrea Stolte for helpful conversations and useful comments on the manuscript, and an anonymous referee for a helpful review. Support for this work was provided by NSF grant AST 04-06816. The W. M. Keck Observatory is operated as a scientific partnership among the California Institute of Technology, the University of California, and the National Aeronautics and Space Administration. The Observatory was made possible by the generous financial support of the W. M. Keck Foundation. The authors wish to recognize and acknowledge the very significant cultural role and reverence that the summit of Mauna Kea has always had within the indigenous Hawaiian community. We are most fortunate to have the opportunity to conduct observations from this mountain.

REFERENCES

Abbott, D. C., & Conti, P. S. 1987, ARA&A, 25, 113
Bauer, M. 2005, Ap&SS, 296, 255
Blackwell, D. E., & Lynas-Gray, A. E. 1994, A&A, 282, 899
Blum, R. D., Ramírez, S. V., Sellgren, K., & Olsen, K. 2003, ApJ, 597, 323
Blum, R. D., Sellgren, K., & DePoy, D. L. 1996a, ApJ, 470, 864
———. 1996b, AJ, 112, 1988
Christou, J. C. 1991, PASP, 103, 1040
Clark, J. S., Larionov, V. M., & Arkharov, A. 2005, A&A, 435, 239
Clénet, Y., et al. 2004, A&A, 417, L15
Cohen, R. E., Herbst, W., & Williams, E. C. 2004, AJ, 127, 1602
Cox, A. N. 2000, Allen's Astrophysical Quantities (4th ed.; New York: AIP)
Cuadra, J., Nayakshin, S., & Sunyaev, R. 2003, A&A, 411, 405
de Jager, C., & Nieuwenhuijzen, H. 1987, A&A, 177, 217
DePoy, D. L., Pepper, J., Pogge, R. W., Stutz, A., Pinsonneault, M., & Sellgren, K. 2004, ApJ, 617, 1127
Depoy, D. L., & Sharp, N. A. 1991, AJ, 101, 1324
Diolaiti, E., Bendinelli, O., Bonaccini, D., Close, L., Currie, D., & Parmeggiani, G. 2000, A&AS, 147, 335
Djurašević, G., Rovithis-Livaniou, H., & Rovithis, P. 2000, A&A, 364, 543
Dworetsky, M. M. 1983, MNRAS, 203, 917
Eisenhauer, F., et al. 2005, ApJ, 628, 246
Figer, D. F. 2004, in ASP Conf. Ser. 322, The Formation and Evolution of Massive Young Star Clusters, ed. H. J. G. L. M. Lamers, L. J. Smith, & A. Nota (San Francisco: ASP), 49

Figer, D. F., et al. 2003, ApJ, 599, 1139
Genzel, R., Pichon, C., Eckart, A., Gerhard, O. E., & Ott, T. 2000, MNRAS, 317, 348
Genzel, R., et al. 2003, ApJ, 594, 812
Ghez, A. M., Klein, B. C., Morris, M., & Becklin, E. E. 1998, ApJ, 509, 678
Ghez, A. M., Morris, M., Becklin, E. E., Tanner, A., & Kremenek, T. 2000, Nature, 407, 349
Ghez, A. M., Salim, S., Hornstein, S. D., Tanner, A., Lu, J., Morris, M., Becklin, E. E., & Duchêne, G. 2005a, ApJ, 620, 744
Ghez, A. M., et al. 2003, ApJ, 586, L127
———. 2005b, ApJ, 635, 1087
Gould, A., & Quillen, A. C. 2003, ApJ, 592, 935
Grenier, S., Gomez, A. E., Jaschek, C., Jaschek, M., & Heck, A. 1985, A&A, 145, 331
Habing, H. J. 1996, A&A Rev., 7, 97
Hornstein, S. D. 2006, Ph.D. thesis, Univ. California, Los Angeles
Hornstein, S. D., Ghez, A. M., Tanner, A., Morris, M., Becklin, E. E., & Wizinowich, P. 2002, ApJ, 577, L9
Humphreys, R. M., & Davidson, K. 1994, PASP, 106, 1025
Lafler, J., & Kinman, T. D. 1965, ApJS, 11, 216
Krabbe, A., Genzel, R., Drapatz, S., & Rotaciuc, V. 1991, ApJ, 382, L19
Krabbe, A., et al. 1995, ApJ, 447, L95
Lefèvre, L., et al. 2005, MNRAS, 360, 141
Lomb, N. R. 1976, Ap&SS, 39, 447
Lu, J. R., Ghez, A. M., Hornstein, S. D., Morris, M., & Becklin, E. E. 2005, ApJ, 625, L51
Martins, F., et al. 2006, ApJ, 649, L103
Mason, B. D., Gies, D. R., Hartkopf, W. I., Bagnuolo, W. G., ten Brummelaar, T., & McAlister, H. A. 1998, AJ, 115, 821
Massey, P. 2003, ARA&A, 41, 15
Matthews, K., Ghez, A. M., Weinberger, A. J., & Neugebauer, G. 1996, PASP, 108, 615
Matthews, K., & Soifer, B. T. 1994, in Infrared Astronomy with Arrays: The Next Generation, ed. I. McLean (Dordrecht: Kluwer), 239
Mennickent, R. E., Vogt, N., & Sterken, C. 1994, A&AS, 108, 237
Meynet, G., & Maeder, A. 2005, A&A, 429, 581
Moffat, A. F. J., Lamontagne, R., Williams, P. M., Horn, J., & Seggewiss, W. 1987, ApJ, 312, 807
Moffat, A. F. J., Poitras, V., Marchenko, S. V., Shara, M. M., Zurek, D. R., Bergeron, E., & Antokhina, E. A. 2004, AJ, 128, 2854
Monnier, J. D., Tuthill, P. G., & Danchi, W. C. 1999, ApJ, 525, L97
Mužič, K., Eckart, A., Schödel, R., & Zensus, A. 2006, in IAU Symp. 238, Black Holes: From Stars to Galaxies—Across the Range of Masses, ed. V. Karas & G. Matt (Cambridge: Cambridge Univ. Press), 140
Nayakshin, S., Cuadra, J., & Sunyaev, R. 2004, A&A, 413, 173
Nayakshin, S., & Sunyaev, R. 2003, MNRAS, 343, L15
Ott, T. 2003, Ph.D. thesis, Max-Planck-Institut für Extraterrestrische Physik
Ott, T., Eckart, A., & Genzel, R. 1999, ApJ, 523, 248
Paumard, T., Genzel, R., Maillard, J. P., Ott, T., Morris, M. R., Eisenhauer, F., & Abuter, R. 2004a, Young Local Universe, ed. A. Chalabaev et al. (Paris: Ed. Frontières), 377
Paumard, T., Maillard, J.-P., & Morris, M. 2004b, A&A, 426, 81
Paumard, T., Maillard, J. P., Morris, M., & Rigaut, F. 2001, A&A, 366, 466
Paumard, T., et al. 2006, ApJ, 643, 1011
Pavlovski, K., Harmanec, P., Bozic, H., Koubsky, P., Hadrava, P., Kriiz, S., Ruzic, Z., & Stefl, S. 1997, A&AS, 125, 75
Peeples, M. S., Bonanos, A. Z., DePoy, D. L., Stanek, K. Z., Pepper, J., Pogge, R. W., Pinsonneault, M. H., & Sellgren, K. 2007, ApJ, 654, L61
Percy, J. R., & Bakos, A. G. 2001, PASP, 113, 748
Press, W. H., Teukolsky, S. A., Vetterling, W. T., & Flannery, B. P. 1992, Numerical Recipes in C (2nd ed.; Cambridge: Cambridge Univ. Press)
Reid, M. J. 1993, ARA&A, 31, 345
Scargle, J. D 1982, ApJ, 263, 835
Schödel, R., Ott, T., Genzel, R., Eckart, A., Mouawad, N., & Alexander, T. 2003, ApJ, 596, 1015
Simons, D. A., & Becklin, E. E. 1996, AJ, 111, 1908
Sterken, C., & Jaschek, C. 1996, Light Curves of Variable Stars: A Pictorial Atlas (Cambridge: Cambridge Univ. Press)
Stetson, P. B. 1996, PASP, 108, 851
Stothers, R. B., & Chin, C.-W. 1996, ApJ, 468, 842
Tamura, M., Werner, M. W., Becklin, E. E., & Phinney, E. S. 1996, ApJ, 467, 645
Theodossiou, E., & Danezis, E. 1991, Ap&SS, 183, 91
Trippe, S., et al. 2006, A&A, 448, 305
Tuthill, P. G., Monnier, J. D., & Danchi, W. C. 1999, Nature, 398, 487
Vacca, W. D., Garmany, C. D., & Shull, J. M. 1996, ApJ, 460, 914
van der Hucht, K. A. 2001, NewA Rev., 45, 135
van der Hucht, K. A., Williams, P. M., & Morris, P. W. 2001, in The Promise of the Herschel Space Observatory, ed. G. L. Pilbratt et al. (ESA SP-460; Noordwijk: ESA), 273
Veen, P. M., van der Hucht, K. A., Williams, P. M., Catchpole, R. M., Duijsens, M. F. J., Glass, I. S., & Setia Gunawan, D. Y. A. 1998, A&A, 339, L45
Voshchinnikov, N. V. 2002, in Optics of Cosmic Dust, ed. G. Videen & M. Kocifaj (Dordrecht: Kluwer), 1
Wegner, W. 1994, MNRAS, 270, 229
———. 2006, MNRAS, 371, 185
Welch, D. L., & Stetson, P. B. 1993, AJ, 105, 1813
White, R. L., & Becker, R. H. 1995, ApJ, 451, 352
Williams, P. M., & van der Hucht, K. A. 1992, in ASP Conf. Ser. 22, Non-isotropic and Variable Outflows from Stars, ed. L. Drissen, C. Leitherer, & A. Nota (San Francisco: ASP), 269
———. 2000, MNRAS, 314, 23
Williams, P. M., van der Hucht, K. A., & Rauw, G. 2005, in Massive Stars and High-Energy Emission in OB Associations, ed. G. Rauw et al. (Liège: Univ. Liège), 65
Williams, P. M., van der Hucht, K. A., & The, P. S. 1987, A&A, 182, 91
Zahn, J.-P. 1977, A&A, 57, 383